

# Gas-Mediated Impact Dynamics in Fine-Grained Granular Materials

John R. Royer,<sup>1</sup> Eric I. Corwin,<sup>1</sup> Peter J. Eng,<sup>1,2</sup> and Heinrich M. Jaeger<sup>1</sup>

<sup>1</sup>*James Franck Institute and Department of Physics, The University of Chicago, Chicago, IL 60637*

<sup>2</sup>*Consortium for Advanced Radiation Sources, The University of Chicago, Chicago, IL 60637*

(Dated: May 26, 2019)

Non-cohesive granular media exhibit complex responses to sudden impact that often differ from those of ordinary solids and liquids. We investigate how this response is mediated by the presence of interstitial gas between the grains. Using high-speed x-ray radiography we track the motion of a steel sphere through the interior of a bed of fine, loose granular material. We find a crossover from nearly incompressible, fluid-like behavior at atmospheric pressure to a highly compressible, dissipative response once most of the gas is evacuated. We discuss these results in light of recent proposals for the drag force in granular media.

PACS numbers: 45.70.Cc, 47.56.+r, 83.80.Fg, 83.10.Tv

Studies of the impact of solid objects into granular beds have a long history, with first systematic work dating back to the 18th century [1, 2]. The topic reemerged in the 1960's with attempts to characterize the mechanical strength of the lunar surface [3, 4] and, recently, with investigations of impact cratering [5, 6, 7, 8, 9, 10, 11, 12, 13] and granular jet formation [14, 15, 16, 17]. One unresolved issue remains the functional form for the drag force experienced by the impacting solid as it moves through the granular medium. Various competing force laws have been proposed, based on scaling laws relating the penetration depth to the impact energy or momentum [5, 6], or on direct measurement of the trajectory of the impacting object [7, 8, 9, 10, 11]. However, none of these take into account the interaction between the solid grains inside a granular bed and the surrounding gas.

This interaction is known to play a significant role in many situations where the bed is externally forced, especially for small grain sizes, when the bed's gas permeability becomes sufficiently low to sustain a pressure gradient that can compete with the weight of the material. The resulting feedback between grain motion and ambient gas flow gives rise to complex dynamics not only when a bed is fluidized by direct gas injection [18], but also in many vibrated granular systems [19, 20, 21, 22]. There have been indications that the morphology of impact craters differs for small grain sizes due to interstitial gas flows [13]. Also, for fine powders, the size and shape of granular jets ejected vertically upward after impact was found to depend on the presence of interstitial gas [16]. However, with one exception [17], the role of gas-grain interactions in determining the trajectory of impacting solids has not been investigated in detail. Here we demonstrate that ambient gas inside a granular bed strongly affects the impact dynamics and show how this alters the drag force in a fine-grained granular medium.

Previous experiments used either two-dimensional (2D) set-ups [11] or indirect methods to gauge the motion of a projectile inside a 3D bed [5, 6, 7, 8, 9, 10]. In con-

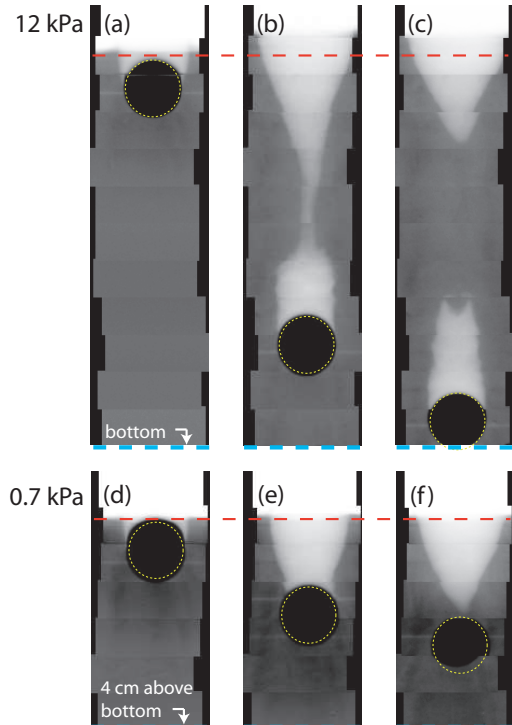


FIG. 1: (Color Online). Pressure dependence of impact dynamics. Composite x-ray images at 12 kPa (a) 5 ms, (b) 40 ms and (c) 57 ms after impact. Images at 0.7 kPa (d) 5 ms, (e) 12 ms and (f) 28 ms after impact. Thin dashed lines indicate the top surface of the bed prior to impact.

trast, our approach is based on high-speed x-ray imaging which gives direct, time-resolved access to the dynamics in the bed interior and also allows us to extract local changes in the bed packing density.

For the experiments reported here, a steel sphere (diameter  $D_s = 12\text{mm}$ ) was dropped from a fixed height of 0.34 m into an 85 mm deep bed of boron carbide ( $B_4C$ ) particles (50  $\mu\text{m}$  avg. diameter).  $B_4C$ , which is non-spherical, was chosen to optimize the x-ray transmission; separate experiments, studying jet formation in a vari-

ety of different media, indicate that grain shape is not a critical parameter [16, 23]. The bed was contained in a cylindrical polycarbonate tube with 35 mm inner diameter. Before each drop the bed was aerated from below by dry nitrogen entering through a diffuser built into the bottom of the container. By slowly turning off the nitrogen flow, the packing fraction  $\phi = V_g/V_{tot}$ , where  $V_g$  is volume occupied by grains and  $V_{tot}$  is the total volume of the bed, was adjusted before each drop to a value around 0.5. The system could be sealed and evacuated down to pressures as low as 0.7 kPa. The pump speed was limited to prevent air from bubbling up and disturbing the loose packing.

X-ray imaging was performed at the GeoSoilEnviro-CARS beamline at the Advanced Photon Source using a high intensity "pink" beam with energy width 5 keV centered at 22 keV. The x-ray transmission through the bed was imaged off a phosphor screen at 6000 frames per second with resolution of  $29 \mu\text{m}/\text{pixel}$  using a Phantom v7 video camera. The beam size restricted the field of view to  $22 \text{ mm} \times 8.7 \text{ mm}$  sections of the bed. To capture the dynamics across the full vertical extent of the bed, movies of multiple independent drops, imaged at different, slightly overlapping vertical bed positions, were stitched together using the passage of the sphere to align them horizontally and synchronize them.

The measured intensity,  $I$ , reaching the detector is a function of the product  $\rho\phi l$ . Here  $\rho$  is the specific density of the grain material and  $l$  the x-ray path length through the bed, as determined from the cylindrical geometry of the set-up. To correct for spatial variations in beam intensity and camera sensitivity, calibration curves relating  $I$  to the packing fraction  $\phi$  were calculated for each of the  $780 \times 300$  pixels in the field of view [23]. Across each frame in a single movie, initial packing fraction  $\phi_0$  varied by about 1%, indicating a very high uniformity of the bed configuration prior to impact. From drop to drop  $\phi_0$  varied between 0.49 and 0.52. This variation in  $\phi_0$  was present at atmospheric pressure, where the pump was disconnected, as well as at reduced pressure, indicating that it was due to small, unavoidable differences in bed settling after fluidization, but not due to the evacuation of the chamber.

X-ray images of the interior reveal a striking air pressure dependence of both bed and sphere dynamics (Fig. 1). At atmospheric pressure ( $P = 101 \text{ kPa}$ ), the sphere easily penetrates the bed, reaching the bottom of the system and opening up a large cylindrical hole. This hole closes first at some intermediate depth, resulting in a crater near the top and a gas-filled cavity behind the sphere. Both of these region then fill in from the sides due to gravitational pressure. This process has previously been identified as driving jet formation [15, 16], but the role of the interstitial gas has remained controversial [17]. At  $P = 12 \text{ kPa}$  the overall features are still similar to those at atmospheric conditions, but the dynamics be-

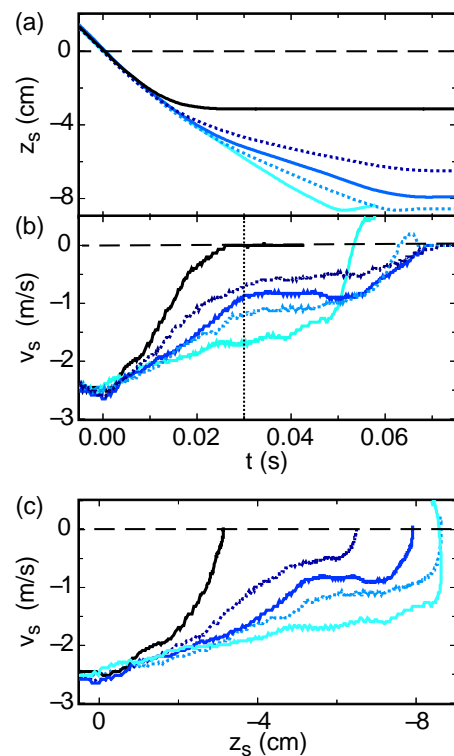


FIG. 2: (Color Online). (a) Vertical position  $z_s$  of bottom tip of the sphere as function of time after impact (at  $t = 0$  s). (b) Velocity  $v_s(t)$  computed from curves in (a). (c) Velocity  $v_s(z_s)$  as a function of depth. In all panels top to bottom:  $P = 0.7 \text{ kPa}$ ,  $4.9 \text{ kPa}$ ,  $8.7 \text{ kPa}$ ,  $12.0 \text{ kPa}$  and  $101 \text{ kPa}$ .

gin to change. The cavity is smaller, and while the top surface of the bed still rises to compensate for the change in bed volume, it does not rise quite as high (Fig. 1a-c). Further reducing the pressure to 0.7 kPa significantly changes the dynamics. The bed barely rises, and there is significant compaction of the grains in front of the sphere, as evident in the darker region under the sphere in Fig. 1d-f. As a consequence, the sphere is able to penetrate only a short distance and the hole closes directly above the sphere without forming a separate cavity region.

To quantify this change in impact dynamics we plot in Fig. 2a the position of the bottom of the sphere,  $z_s(t)$ , as it moves through the bed. At  $P = 101 \text{ kPa}$  the sphere hits the bottom with sufficient momentum to bounce back up a bit; at  $P = 8.7 \text{ kPa}$  and below the sphere is stopped well before reaching the bottom. From  $z_s(t)$  we compute  $v_s = dz_s/dt$ , shown in Fig. 2 b, c. With decreasing ambient air pressure there is a monotonic decrease in penetration depth and a concomitant increase in overall resistance of the bed.

Inside the bed the net force on the impacting solid is the sum of its weight,  $-mg$ , and a drag force,  $F_d$ , representing the bed resistance. Models for this resistance are of the form  $F_d = F_C + c|v_s|^\beta$ , where  $F_C$  represents a Coulomb friction term and  $c$  is a parameter characteriz-

ing the strength of a velocity-dependent drag term. Specific forms include  $F_C = \text{const}$  with  $\beta = 1$  [5],  $F_C = \kappa|z_s|$  with  $c = 0$  [8, 10],  $F_C = \kappa|z_s|$  with  $\beta = 2$  [9] as well as models with  $\beta = 2$  but a more complex  $z_s$ -dependence for  $F_C$  [12]. Note that all of these models predict a non-zero deceleration,  $a = -g + F_d/m$ , of the projectile and thus a  $z_s$ -dependence of its velocity over the whole range from impact to final stop.

Inspection of the data in Fig. 2 for intermediate pressures reveals a feature that is not captured by any available model: a region of near-constant velocity. Roughly 30 ms after the impact (dotted vertical line) the sphere enters a regime where it descends at nearly constant speed. This behavior can be seen most clearly when the velocity is plotted as function of depth,  $z_s$ , below the free surface (Fig. 2c). A second important feature is the very rapid deceleration *after* the constant velocity regime, seen clearly in the traces for  $P = 4.9$  kPa and 8.7 kPa. It is nearly as abrupt as when the sphere hits the bottom of the container (see traces for higher pressures), but occurs here sufficiently far inside the bed for boundary effects to be irrelevant [24]. As we show below, these characteristic features are closely linked to the interplay between penetrating sphere, bed particles, and interstitial gas.

X-ray radiography allows us to track this interplay both in front of the moving projectile and by following the movement of material surrounding the void all the way up to the top surface of the bed. In Fig. 3, we plot the change in local packing fraction,  $\Delta\phi = \phi - \phi_0$ , measured along the centerline of the path of the sphere, at three different depths,  $z_m$  below the surface. In vacuum there is a sharp jump in the packing fraction well before the sphere arrives. With increasing depth this front occurs further ahead of the sphere, demonstrating that the compacted region grows: the sphere is plowing into grains which do not readily move out of the way, thus adding to the denser material in front of it. The situation is quite different at atmospheric pressure. Now the packing fraction remains constant except for a slow upturn once the sphere comes to within about half its diameter of  $z_m$ . The width of this small compaction front does not vary much with depth. The overall magnitude of compaction decreases smoothly with increasing pressure (Fig. 3c).

A more global measure of the effect of interstitial gas is the rise of the top level of the bed as the sphere burrows in and starts producing the cavity. This rise can be seen in Figs. 1a-c by comparison with the pre-impact level (horizontal dotted line). A similar rise was observed in experiments studying jet formation in systems with grain sizes  $< 100\mu\text{m}$  [15, 16, 17], but is considerably reduced when the system is evacuated (Figs. 1d-f). In Fig. 4a we track the level change,  $\delta h$ , of the top surface for different pressures. At impact, the bed rapidly rises, then at time  $t_m$  (highlighted for 101 kPa, 8.7 kPa and 0.7 kPa by arrows in Fig. 4a) levels off into a broad maximum of

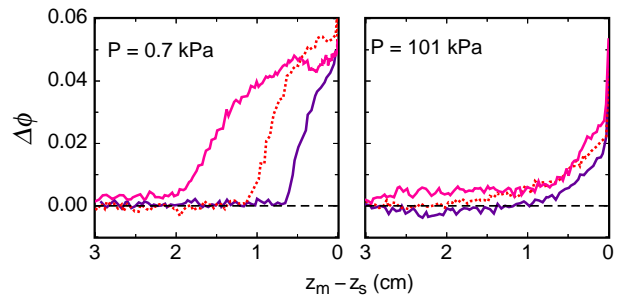


FIG. 3: (Color Online). Compaction fronts preceding sphere. Change in packing fraction  $\Delta\phi$  measured along centerline of path of the sphere at depths (from left to right)  $z_m = 1.0$  cm, 2.0 cm and 3.0 cm plotted against distance from tip of the sphere to  $z_m$  at 101 kPa (left) and 0.7 kPa (right).  $z_m - z_s = 0$  corresponds to tip of the sphere  $z_s$  arriving depth  $z_m$ .

height  $\delta h_{max}$  and eventually falls back. The final level has  $\delta h < 0$  because the impact-induced vibrations compacted the initial, loosely-packed bed (at atmospheric pressure this final settling does not occur until times much later than shown). The change in height  $\delta h_{max}$  increases with pressure, suggesting that the interstitial gas serves to make the bed as a whole less compressible and more fluid-like.

To check this directly, we use x-ray images as in Fig. 1 to track the shape of the cavity over time and estimate its volume, assuming cylindrical symmetry. For atmospheric pressure we find that  $\delta h(t)$  indeed corresponds, within experimental uncertainties, to what would be expected from an incompressible fluid. With decreasing  $P$  the level  $\delta h_{max}$  drops below the value obtained from the cavity volume (double-sided arrows in Fig. 4a), indicating a much less elastic response.

We can characterize the elasticity of the bed by comparing the gravitational energy gained by the bed  $\Delta U_b$  to the kinetic energy lost by the sphere  $\Delta K_s$  in time  $t_m$ . While at  $P = 0.7$  kPa only 0.1% of the impacting sphere's energy is transferred to the bed this value increases to about 45% at atmospheric pressure (Fig. 4b). This can be compared to values around 10% found in 2D simulations without interstitial gas [12].

To understand the fluid-like behavior at large  $P$  we consider the gas permeability of the bed. Pressure differences capable of supporting weight can build up in porous media if the timescale for gas to diffuse out of the bed is significantly longer than the timescale of the granular flow. The diffusion constant for gas with viscosity  $\mu$  flowing through a bed of permeability  $k$  is  $D = \frac{kP}{\mu(1-\phi)}$ . For our experimental conditions  $D \sim 5$  cm<sup>2</sup>/s at  $P = 101$  kPa. The timescale to diffuse across the depth of our bed (a distance  $L = 8.5$  cm), is  $\tau_D = L^2/D \sim 140$  ms, significantly longer than the time  $t_m \sim 30$  ms for the bed to rise to  $\delta h_m$  (dotted vertical line in Fig. 4a). This is consistent with air being trapped in the bed interstices and

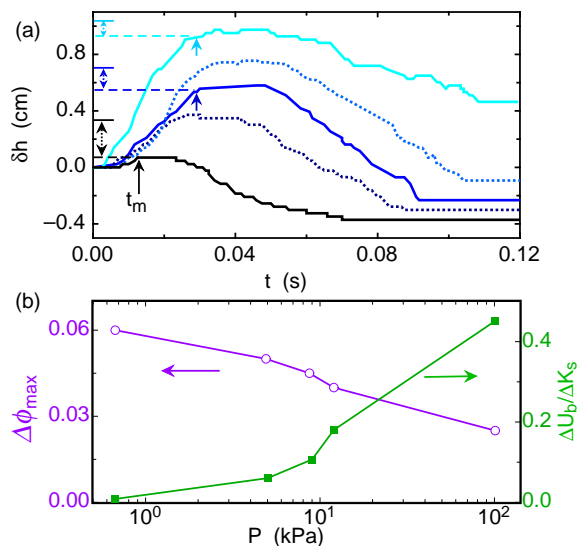


FIG. 4: (Color Online). Bed dynamics. (a) Rise of bed top surface. Bottom to top:  $P = 0.7$  kPa, 4.9 kPa, 8.7 kPa, 12.0 kPa and 101 kPa. Arrows mark location of  $t_m$  for three pressures. Double-sided arrows denote rise needed to conserve bed volume without compaction. (b) Maximum change in packing fraction in front of sphere ( $\circ$ ) and ratio of potential energy needed to raise bed by  $\delta h_{\max}$  to kinetic energy lost by sphere at time  $t_m$  ( $\blacksquare$ ).

preventing compaction. Since the permeability depends on the grain diameter according to  $k \sim d^2$  [21], this cushioning effect would be less pronounced with larger grains, as noted in [3]. Conversely, we expect the behavior observed for larger grains to resemble that found at our lowest pressures. Indeed, the trajectory and velocity of the sphere at 0.7 kPa is qualitatively similar to trajectories measured by Durian et al. in  $250\mu\text{m} - 350\mu\text{m}$  glass spheres [6, 9].

The air-mediated dynamic response of the granular bed directly affects the drag experienced by the impacting sphere. Comparing Figs. 4a and 2b,c we see that the onset of the constant speed regime coincides with  $t_m$ , the start of the plateau in bed level rise. During this plateau stage the material displaced by the sphere is flowing mostly into the cavity behind it. Consequently, the sphere in this regime is affected not by the full bed, but instead by a more local region. For  $v_s \sim 1$  m/s, as for our data, the drag  $\phi\rho D_s^2 v_s^2$  is within a factor of two of the weight of the sphere. Inside the observed regime of constant velocity this then suggests a large reduction, and possible vanishing, of  $F_C$  in the force law. When the top level of the bed begins to fall again, the cavity behind the sphere has pinched shut (Fig. 1c), trapping an air pocket below the surface [16]. With the falling bed and trapped air pocket, the bed material is no longer free to flow out of the way of the sphere. Therefore, Coulomb friction is again set by the full weight of the bed, resulting in a sudden increase in  $F_C$  that quickly decelerates

the sphere and brings it to rest.

As a result, a friction term of the form  $F_C = \kappa|z|$  cannot capture the full range of observed behavior, even if  $\kappa$  is made to depend on pressure. Such pressure dependence was very recently proposed by Cabarellero *et al.* [17] who measured the trajectory of a sphere impacting  $40\mu\text{m}$  sand by tracking a string attached to it. Our results agree with their conclusion that the shallower penetration at lower pressures is due to increased friction. However, since  $\Delta\phi > 0$  (Fig. 3) at all pressures, drag reduction is not simply due to fluidization of grains ahead of the sphere. Instead, our measurements of the local packing fraction indicate that in the presence of air the bed as a whole behaves more like an incompressible fluid, allowing the impacting sphere to penetrate deep and create a large cavity. In the absence of air the bed compacts much more strongly ahead of the sphere, rapidly dissipating energy and decelerating the descent.

We thank B. Conyers, M. Rivers, M. Möbius and S. Nagel for insightful discussions, and D. Durian and D. Lohse for sharing their results prior to publication. This work was supported by NSF through its MRSEC program under DMR-02137452. GSECARS is supported by NSF EAR-0217473, DOE DE-FG02-94ER14466, the State of Illinois and the W. M. Keck Foundation. Use of the Advanced Photon Source was supported by DOE-BES under W-31-109-Eng-38.

- 
- [1] B. Robins, *New Principles of Gunnery* (London, 1742).
  - [2] J. V. Poncelet, *Introduction à la mécanique industrielle, physique ou expérimentale* (Paris, 1839).
  - [3] J. R. C. Garry, M. C. Towner, A. J. Ball, J. C. Zarnecki, and G. Marcou, *Adv. Space Res.* Vol. 23, No. 7, 1229-1234 (1999).
  - [4] D. J. Roddy, J. B. Rittenhouse and R. F. Scott, *AIAA J.* **1** (4), 868-873 (1963).
  - [5] J. R. de Bruyn, and A. M. Walsh, *Can J. Phys.* **82**, 439 (2004).
  - [6] J. S. Uehara, M. A. Ambroso, R. P. Ojha and D. J. Durian, *Phys. Rev. Lett.* **90**, 194301 (2003); **91**, 149902(E) (2003).
  - [7] M. A. Ambroso, R. D. Kamien, and D. J. Durian, *Phys. Rev. E* **72**, 041305 (2005).
  - [8] D. Lohse, R. Rauhe, R. Bergmann, and D. van der Meer, *Nature* **432**, 689-690 (2004).
  - [9] H. Katsuragi and D. J. Durian (preprint 2006).
  - [10] M. Hou, Z. Peng, R. Liu, K. Lu, and C. K. Chan, *Phys. Rev. E* **72**, 062301 (2005).
  - [11] M. P. Ciamarra, A. H. Lara, A. T. Lee, D. I. Goldman, I. Vishik and H. L. Swinney, *Phys. Rev. Lett.* **92**, 194301 (2004).
  - [12] L. S. Tsimring and D. Volfson, *Powders and Grains 2005*, eds. Garcia-Rojo, Herrmann and McNamara (Balkema, Rotterdam, 2005), p. 1215.
  - [13] A. M. Walsh, K. E. Holloway, P. Habdas, and J. R. de Bruyn, *Phys. Rev. Lett.* **91**, 104301 (2003).
  - [14] S. T. Thoroddsen, and A. Q. Shen, *Physics Of Fluids* **13**,

- 4-6 (2001).
- [15] D. Lohse, R. Bergmann, R. Mikkelsen, C. Zeilstra, D. van der Meer, M. Versluis, K. van der Weele, M. van der Hoef and H. Kuipers, *Phys. Rev. Lett.* **93**, 198003 (2004).
- [16] J. R. Royer, E. I. Corwin, A. Flior, M.-L. Cordero, M. L. Rivers, P. J. Eng and H. M. Jaeger, *Nature Physics* **1**, 164 (2005).
- [17] G. Caballero, R. Bergmann, D. van der Meer, A. Prosperetti, and D. Lohse, in preparation.
- [18] R. Jackson, *The Dynamics of Fluidized Particles* (Cambridge University Press, 2000).
- [19] R. G. Gutman, *Chem. Eng. Sci.* **30**, 89 (1975).
- [20] H. K. Pak, E. VanDoorn, and R. P. Behringer, *Phys. Rev. Lett.* **74**, 4643-4646 (1995).
- [21] M. E. Möbius, X. Cheng, G. S. Karczmar, S. R. Nagel, and H. M. Jaeger, *Phys. Rev. Letters* **93**, 198001 (2004).
- [22] N. Burtally, P. J. King, P. J. M. R. Swift, *Science* **295**, 1877-1879 (2002).
- [23] J. R. Royer, E. I. Corwin, B. Conyers, A. Flior, P. J. Eng, H. M. Jaeger, in preparation.
- [24] M. B. Stone, D. P. Bernstein, R. Barry, M. D. Pele, Y. Tsui and P. Schiffer, *Nature* **427**, 503-504 (2004).